
Article:
Jin, H., Ghazizadeh, S. and Provis, J.L. orcid.org/0000-0003-3372-8922 (2025) Investigation of alkali-silica reaction in alkali activated cements by thermodynamic modelling. Materials and Structures, 58 (8). 265. ISSN: 1359-5997

https://doi.org/10.1617/s11527-025-02781-z

Materials and Structures (2025) 58:265
https://doi.org/10.1617/s11527-025-02781-z

ORIGINAL ARTICLE

Investigation of alkali-silica reaction in alkali activated cements by thermodynamic modelling

Haoliang Jin · Sam Ghazizadeh · John L. Provis

Received: 20 February 2025 / Revised: 26 June 2025 / Accepted: 24 August 2025

Abstract The likelihood and consequences of the alkali-silica reaction (ASR) in mortars and concretes based on alkali-activated materials (AAMs) are still under discussion, due largely to the characteristically high alkali levels of this class of cements. In this study, applying thermodynamic modelling to the study of ASR provides a new insight into ASR mechanisms as a function of binder chemistry. By considering different activators (NaOH, Na_2SO_4, Na_2CO_3, $Na_2O.nSiO_2$ with various values of the modulus n) at different dosages, the volume of shlykovite-type ASR products that can potentially form in AAMs with partially reactive siliceous aggregates was calculated. The solution chemistry and phase assemblage after hydration provide further information to aid in explaining the observed trends. Although high concentrations of Na-bearing activators were used in the AAM formulations, much less Na-shlykovite and no K-shlykovite are formed, compared to Portland cement. The volume of Na-shlykovite formed decreases with an increase in the dosage of activators (for all activators tested), and with a decrease in the modulus of sodium silicate when this is the activator used. A high concentration of Ca after hydration, rather than the concentration of alkalis in the pore solution, is the controlling factor in shlykovite formation, which represents ASR in these simulations.

Keywords Alkali-silica reaction · Alkali activated cement · Activators · Thermodynamic modelling

1 Introduction

The alkali-silica reaction (ASR) is an important mechanism of degradation in some concretes; opinions regarding whether this is a major problem in alkali-activated materials (AAMs) are divided, and this topic requires further attention. Alkali sources (mainly, but not solely, from the paste) and reactive silicates in the aggregates are the essential factors triggering the process of ASR in the presence of available calcium and moisture, forming expansive ASR gels. Because of the very high content of alkalis present in AAMs, which can be an order of magnitude higher than the levels conventionally considered "safe" in Portland cement, some researchers have proposed on this basis that AAMs may be expected to be more susceptible to ASR than Portland cement [1–3].

H. Jin · J. L. Provis
Department of Materials Science and Engineering, The University of Sheffield, Sheffield, UK
e-mail: 414109471@qq.com

S. Ghazizadeh
Special Services, Mott MacDonald, London, UK
e-mail: sam.ghazizadeh@mottmac.com

J. L. Provis (✉)
PSI Center for Nuclear Engineering and Sciences, Paul Scherrer Institut, Forschungsstrasse 111, 5232 Villigen, Switzerland
e-mail: john.provis@psi.ch

Published online: 19 September 2025

On the other hand, experimental evidence tends not to fulfil those predictions. In an early study, Gifford and Gillott [4] stated that there is less expansion caused by ASR in AAMs than in conventional mortars. This observation was supported by the work of García-Lodeiro et al. [5], and also by the early European work summarised in the review of Talling and Brandstetr [6]. Those authors attributed the ASR resistance of AAMs to the hydration products containing and binding more of the alkalis. More recently, Wang et al. [7] investigated ASR in alkali-activated binders produced from a blend of slag and fly ash, and gave the conclusion that dissolved reactive silicates were consumed to form hydration products, which combined with autogenous shrinkage during hydration, was proposed to inhibit the process of ASR. The factors that affect ASR in AAMs have been reviewed in detail in [8, 9] and in several other studies, leading to an understanding that low-calcium AAMs tend to show less ASR than their higher-calcium counterparts [10], and that further development of testing methods is needed to ensure that representative results are obtained in any comparison between AAM binder types, or against a Portland cement baseline [11].

The conclusion of this assessment is that, due to the variation in the composition of precursors, activators, and testing methods used in the experiments that have been provided in the literature, and the lack of clarity about fundamental mechanisms at a physicochemical level, more comprehensive research studies should be designed to gain a deeper understanding of the mechanism and implications of ASR in AAMs. The intention of the current study is to provide theoretical insight in support of the experimental campaigns that are ongoing, by assessing the thermodynamic basis for ASR processes in AAMs.

The extensive development of the cementitious hydrate phase database for thermodynamic modelling in recent years has enabled researchers to computationally predict the formation and composition of both solid and liquid phase assemblages, for both Portland-based cements and alkali-activated cements. For example, Lothenbach and co-workers reviewed the applications of thermodynamic modelling in the cement science and pointed out some potential examples that can be solved using this method [12, 13]. Importantly for the modelling of AAMs, Myers et al. [14] proposed a new solid solution model to establish the database for sodium/aluminium-substituted calcium silicate hydrate (C-N-A-S–H). Kulik et al. [15, 16] have also contributed very important insight into the thermodynamics of calcium silicate hydrate phases when incorporating aluminium, and alkalis such as sodium and potassium. These updated models allow improved prediction of phase formation and stability in the AAM system. In terms of modelling ASR, the limited thermochemical or solubility data available for some relevant potential ASR products, as well as the ongoing discussion of what exactly is the structure of the ASR gel formed under different circumstances, has been an obstacle in the development of thermodynamic modelling applications in this area, for both Portland and AAM cements. However, in an important recent advance, Shi et al. [17] successfully synthesised shlykovite-type ASR products at 80 °C, and thereafter their thermodynamic parameters were calculated by Jin et al. [18]. This type of advancement in material characterisation and database development, supported by modelling approaches allowing the separation of timescales between successive reaction processes (hydration and ASR), has made thermodynamic modelling more soundly-based as a tool for ASR prediction, as demonstrated in [19] for the case of Portland blended cements. More recently, Razki et al. [20] further updated the thermodynamic dataset for nanocrystalline products (ASR-P1) and contributed to the understanding of expansion mechanisms, verifying the importance and effectiveness of thermodynamic modelling in assessing the potential for ASR damage.

The aim of this paper is to investigate ASR processes in AAMs using thermodynamic modelling, focusing on phase evolution at ambient temperature (25 °C) to simulate field exposure conditions. AAMs based on ground granulated blast furnace slag (GGBFS) with different activators (NaOH, Na_2SO_4, $Na_2O{\bullet}nSiO_2$, Na_2CO_3) with different dosage and modulus will be considered in terms of the volume of ASR products formed, compared with Portland cement as a baseline case. Information about pore solution chemistry and phase assemblages before the process of ASR is also used to explain the effects of these factors on the formation of ASR products. These modelling results can be used as a baseline when studying ASR in AAMs, in support of (and to aid design of) long-term or accelerated experiments in the future.

2 Materials and methods

2.1 Materials

The chemical composition of GGBFS used in the study is shown in Table 1, and is reproduced from the work of Mundra et al. [21] who also used this slag composition to model AAMs for chloride transport prediction. A 60% degree of reaction of the GGBFS has also been adopted here based on their research, to represent the long-term characteristics of a relatively mature binder; the potential effects of variations in precursor and activator composition and reactivity are not explicitly included, but offer scope for future research. The consumption of portlandite and the release of alkali ions left in the pore solution are defined as driving the process of ASR, reacting with silica supplied by the aggregate. These two factors are directly related to the degree of reaction for Portland cement, but less so in the case of slag-based AAMs because GGBFS contains only a low level of alkalis, and there will be little or no $Ca(OH)_2$ present in AAM systems.

To investigate the difference between AAM and Portland cement (PC) under ASR-generating conditions, the latter (with an assumed 100% degree of hydration) is also considered as a control system in the analysis, and the composition simulated is listed in Table 1, consistent with our previous work on blended cements [19] where we selected a cement composition from [22]. The thermodynamic simulation methodology is based on bulk oxide compositions rather than detailed phase contents of the slag and Portland cement, as the simulations are implemented by calculating the thermodynamic equilibrium state considering all system constituents, irrespective of the form in which they are supplied.

The four activators (NaOH, Na_2SO_4, $Na_2O{\bullet}nSiO_2$, Na_2CO_3) are used with dosages that are set to achieve equivalent Na_2O contents of 2, 4, 6, and 8 g Na_2O per 100 g BBGFS – abbreviated for conciseness as 2, 4, 6, and 8% Na_2O for discussion in the text and graphics. The different modulus values of waterglass (n = 0.5, 1, 1.5, and 2 in the formula $Na_2O{\bullet}nSiO_2$, defined on a molar basis) are considered to evaluate its effect on ASR in waterglass-activated AAM. The water to solids mass ratio is 0.40 for all AAMs, and 0.47 for cement. The mix design information is summarised in Table 2.

2.2 Methods and modelling description

The simulation methodology and software details used in this paper are based on our previous work [19], where a two-step approach to modelling ASR in blended cements was developed and validated. Detailed information is given below.

2.2.1 Software and database

To simulate ionic interactions and phase assemblages during the process of ASR, the GEM-Selektor v.3 software [23] based on minimisation of Gibbs free energy with mass balance constraints was used. The activity coefficients of aqueous species are calculated

Table 1 The composition of GGBFS and Portland cement used in the simulations in this study, expressed as wt% of oxides

	CaO	SiO_2	Al_2O_3	Fe_2O_3	MgO	Na_2O	K_2O	SO_3
GGBFS	42.3	32.3	13.3	0.6	5.2	0	0.3	2.9
PC	63.12	20.47	5.51	2.45	2.82	0.29	1.16	2.6

Table 2 The activator dosages and modulus values of waterglass considered in this study, expressed as equivalent Na_2O% (g Na_2O per 100 g GGBFS); w/s is the water to solids mass ratio

Activators	NaOH	Na_2SO_4	$Na_2O{\bullet}nSiO_2$	Na_2CO_3
Dosage	2,4,6,8%	2,4,6,8%	2,4,6,8%	2,4,6,8%
Modulus (value of *n*)			0.5, 1.0, 1.5, 2.0	
w/s	0.40			

by the Truesdell-Jones form of the extended Debye-Hückel equation, which is shown in Eq. (1):

$$\log_{10}\gamma_i = \frac{-A_\gamma z_i^2\sqrt{I}}{1 + aB_\gamma\sqrt{I}} + b_\gamma I \quad (1)$$

where the coefficients A_γ and B_γ are related to the temperature and pressure of the system, z_i is the charge of species i, and I is the effective molal ionic strength. The parameters a and b_γ are solution-dependent parameters. Assuming that KOH solution is the main aqueous phase in Portland cement, a and b_γ are set to 3.67 Å and 0.123 kg/mol, while in AAMs whose pore fluid is dominated by NaOH, these two values should be set to 3.31 Å and 0.098 kg/mol respectively [24].

The Cemdata18 database covers the thermodynamic data for the solid phases considered in the simulation, while the database entries for two specific ASR products were obtained from our previous work [18] as shown in Table 3. Other types of ASR products are not included here due to lack of proper database entries. For PC systems the CSHQ model is selected for description of C-S-H, while in AAM simulations, the CNASH_ss solid solution model is selected. The compositions of slag and PC are inputted as oxides, while activators are inputted as compounds. Phases in the Cement18 database are included during the simulation, deactivating some phases which are very slow to form at ambient temperature such as gibbsite, thaumasite, hematite, and quartz.

2.2.2 Model description

The two-part reaction sequence used to represent the successive processes of AAM hydration and ASR has been validated in our previous work [19], and we are also applying that approach in the current simulation: we assumes that the process of AAM hydration has reached effective completion (i.e. achieved the specified degree of reaction) before the formation of ASR products commences. This is based on the understanding that ASR is a slow process at room temperature. Therefore, precursor hydration is the main task in the first part of the simulation. The compositions of the GGBFS and activator were inputted into the GEMS software, to predict both the concentrations of ions in the pore solution and the quantities of solid hydrates formed in the hydration process. Ions in the pore solution, and portlandite in Portland cement, have been reported to take significant roles in affecting the process of ASR [25, 26], and so these are used as the potentially reactive constituents in the second stage of the simulations. These alkaline components react with an additional (reactive) silica source representing the dissolution of silica from the aggregate, added at 50 g per 100 g GGBFS hydrated to ensure that it is not fully depleted during the simulation, to simulate the process of ASR, considering the rest of the hydrates to be inert in this process.

Although the high alkalinity of AAM systems may enhance the dissolution of reactive aggregates, it is assumed that no silica dissolves from the aggregates in the initial (fast) stage of the hydration reaction process; the aggregate is only allowed to participate in the second (longer-term) stage of the reaction process once the hydration or alkali-activation simulation is completed.

3 Results

3.1 Phase assemblage

The phase assemblages formed through alkali-activation, i.e. before AAMs are subjected to the simulated ASR process, are shown in Fig. 1. In general, the simulated phases and their volumes are broadly consistent with those obtained from the work of Mundra

Table 3 Thermodynamic properties of two shlykovite-type ASR products [18]

Products	ΔfH° (kJ/mol)	ΔfG° (kJ/mol)	S° (J/mol·K)	Cp° (J/mol·K)	$Log_{10}K$ at 25°C
K-shlykovite: $KCaSi_4O_8(OH)_3{\cdot}2H_2O$	-5163.6 ± 8	-5293.1 ± 3	485.8 ± 48	426.8 ± 42	-31.2 ± 1.2
Na-shlykovite: $NaCaSi_4O_8(OH)_3{\cdot}2.3H_2O$	-5267.5 ± 9	-5364.4 ± 2	435.9 ± 43	382.9 ± 38	-34.8 ± 0.4

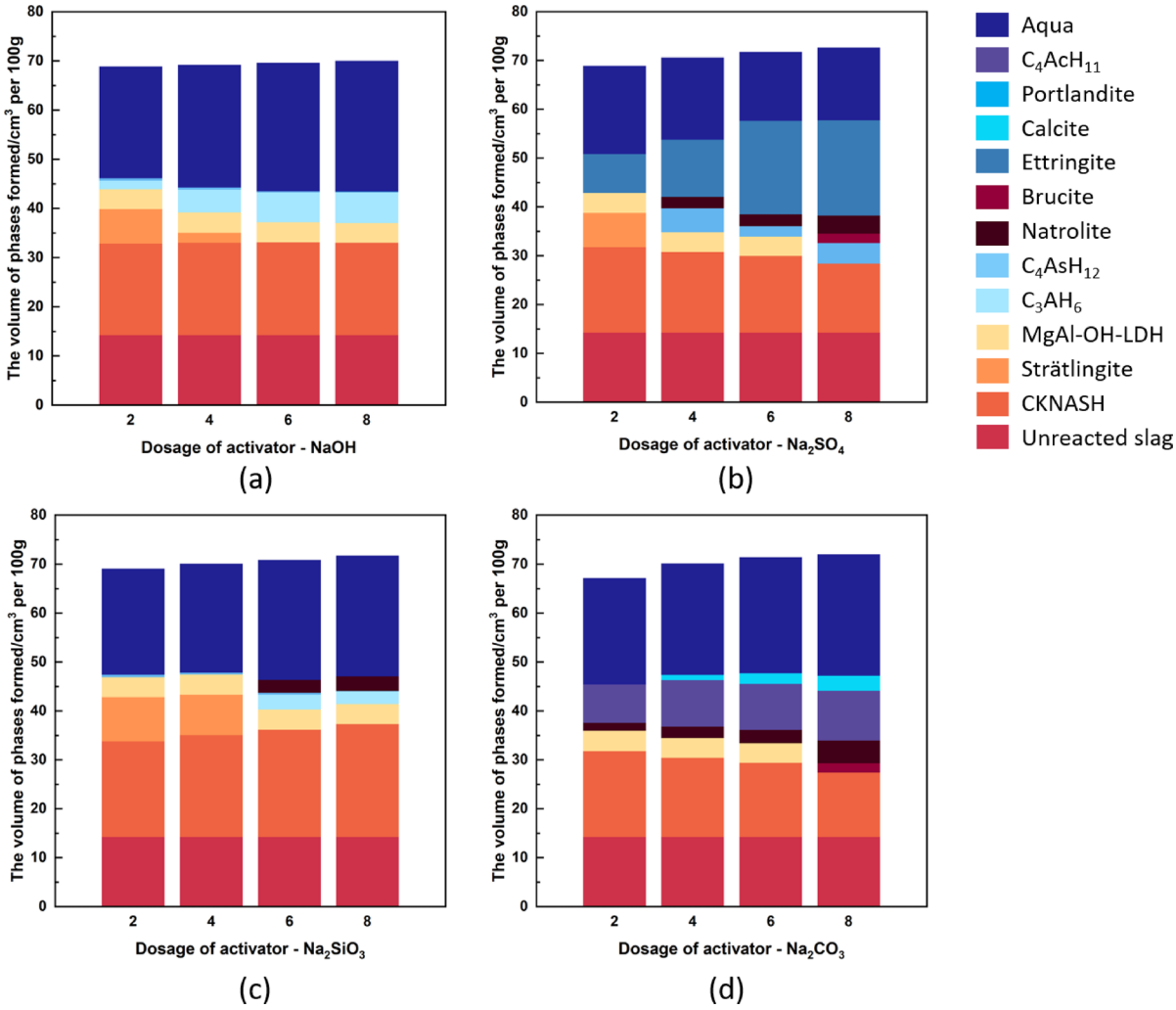

Fig. 1 The simulated phase assemblages resulting from GGBFS activation by four activators with various dosages. The phase "aqua" represents the aqueous pore solution, which is a concentrated electrolyte solution in equilibrium with the newly-formed solid phases

et al. [21] other than some slight differences (for example C_3AH_6 in the NaOH-activated GGBFS and ettringite in the Na_2SO_4-activated GGBFS). The reason for this is due to the updated Cemdata18 database [27] used here, while Mundra et al. [21] used Cemdata14, where changes in the relative stabilities of hydrogarnet phases with respect to other aluminates were a particularly important update that was made between these two database versions [27–29].

In the work of Mundra et al. [21] they focused on the effect of slag composition on phase changes, while here we mainly investigate the influence of dosage of different activators. It can be seen that there is a decrease in the formation of C-(K, N)-A-S–H for Na_2SO_4-activated and Na_2CO_3-activated GGBFS when increasing the activator dosage, but an increase in the secondary hydration products. This results in more Ca being consumed from the pore solution. Likewise, more C_3AH_6 precipitates with higher dosages of the other two activators used. Thus, increasing the dosage of the activator enhances the combination of ions in the pore solution and the formation of solid phases.

For the AAM with the highest dosage of NaOH, portlandite can be seen in Fig. 1a although its volume is quite minor. Brucite is predicted to precipitate in

the activation of GGBFS by Na_2SO_4 and Na_2CO_3 at dosages of 8% equivalent Na_2O, which contrasts with the results of experimental research where there is no brucite formed [30, 31]. The reason for this difference is due to lack of thermodynamic data for low Mg/Al ratio Mg–Al-OH-LDH_ss (Mg–Al layered double hydrates with hydroxide as the sole anion) and M-S–H (magnesium silicate hydrate) [32]. The GGBFS used here contains a high amount of MgO, resulting in the formation of brucite as the Mg is not accommodated in other potential reaction product phases. Natrolite is predicted to form in AAMs, except when NaOH is used as an activator, and appears to be a proxy also for the disordered N-A-S–H type products which form in alkali-activated cements, which have chemical structures and energetics resembling those of zeolites. This zeolite-type product is also predicted to form in the simulation work of Myers et. al and Mundra et. al [21, 32, 33], who reported that the formation of natrolite alongside the calcium-rich hydrous silicates in GEMS simulations indicates the coexistence of C-N-A-S–H gel and N-A-S–H gel. The compositions of the disordered gel products produced in the simulations here are consistent with the findings presented in those papers. The ASR simulations here are relatively insensitive to the exact compositions of the gel phases because the gels are treated as unreactive in the second-stage simulations in which ASR products are formed, beyond their indirect influence via effects of gel chemistry on pore fluid compositions, and so the focus of the discussion here is directly on the pore fluid rather than the hydrate phases.

The phase assemblages of AAMs with different modulus waterglass activators at different equivalent Na_2O doses are shown in Fig. 2. The formation of C-S–H gradually increases when increasing the modulus of waterglass, which is consistent with refs. [21, 32] who considered the effects of Na_2SiO_3 and $Na_2Si_2O_5$ as activators on the phase assemblage of AAM. Strätlingite is predicted to form at lower activator dosages, and also precipitates in the silicate-activated systems shown in Fig. 2c with higher modulus. In turn, the formation of katoite can be seen when there is a relatively low amount of strätlingite (e.g. 0.5% activator dosage in Fig. 2b) or in the absence of strätlingite. Myers et al. [32] stated that it is more likely to form strätlingite in the activation of slags with low or moderate Si contents, and this may be used to explain the absence of this phase at higher silicate activator dosages due to the additional silica present in those cements. However, the reasons for the transformation of strätlingite and katoite may be attributed to the use of different thermodynamic databases between the two studies [27, 34]. The formation of zeolite (natrolite), representing N-A-S–H as noted above, is expected when increasing the modulus and dosage of the silicate activator.

3.2 Pore solution chemistry

Considering the effects of various dosages of the four activators on solution chemistry in AAMs after hydration (stage 1 of the two-step reaction process, before the ASR simulation is initiated), the concentrations of the elements that can participate in formation of ASR products, and hydroxyl ions, in the pore solution are shown in Fig. 3. When increasing the activator dosage, the concentration of Na increases dramatically in all AAM samples. A similar trend is seen with respect to the change of concentration of hydroxyl ions, largely for reasons of charge balance, resulting in a more highly alkaline environment and more new phases formed, which is consistent with the results shown in Fig. 1.

The higher concentration of alkalis in AAMs is sometimes claimed to be a detrimental factor causing a higher risk of formation of ASR products, or alkaline dissolution of the aggregates, compared to Portland cement. The simulation here covers this relationship, which will be discussed in Sect. 3.3. It is also potentially notable that the concentration of hydroxyl ions reduces at an Na_2SO_4 dosage of 8% Na_2O equivalent. This may be attributed to precipitation of brucite (Fig. 1b) which may lead to a decrease in the concentration of hydroxyl ions in the pore solution. However, a different trend was found in Na_2CO_3-activated slag, which also forms brucite at higher dosages; the rise in the concentration of hydroxyl ions with increasing Na_2CO_3 dosage is due to the transformation from Mg–Al-OH-LDH to $Mg(OH)_2$.

Several experimentally-oriented papers have reported the concentrations of elements in the pore solution of AAMs, either as a function of curing time, or with different dosages of waterglass or NaOH activators [35–38]. The near-neutral salt activators Na_2CO_3 and Na_2SO_4 have slower hydration

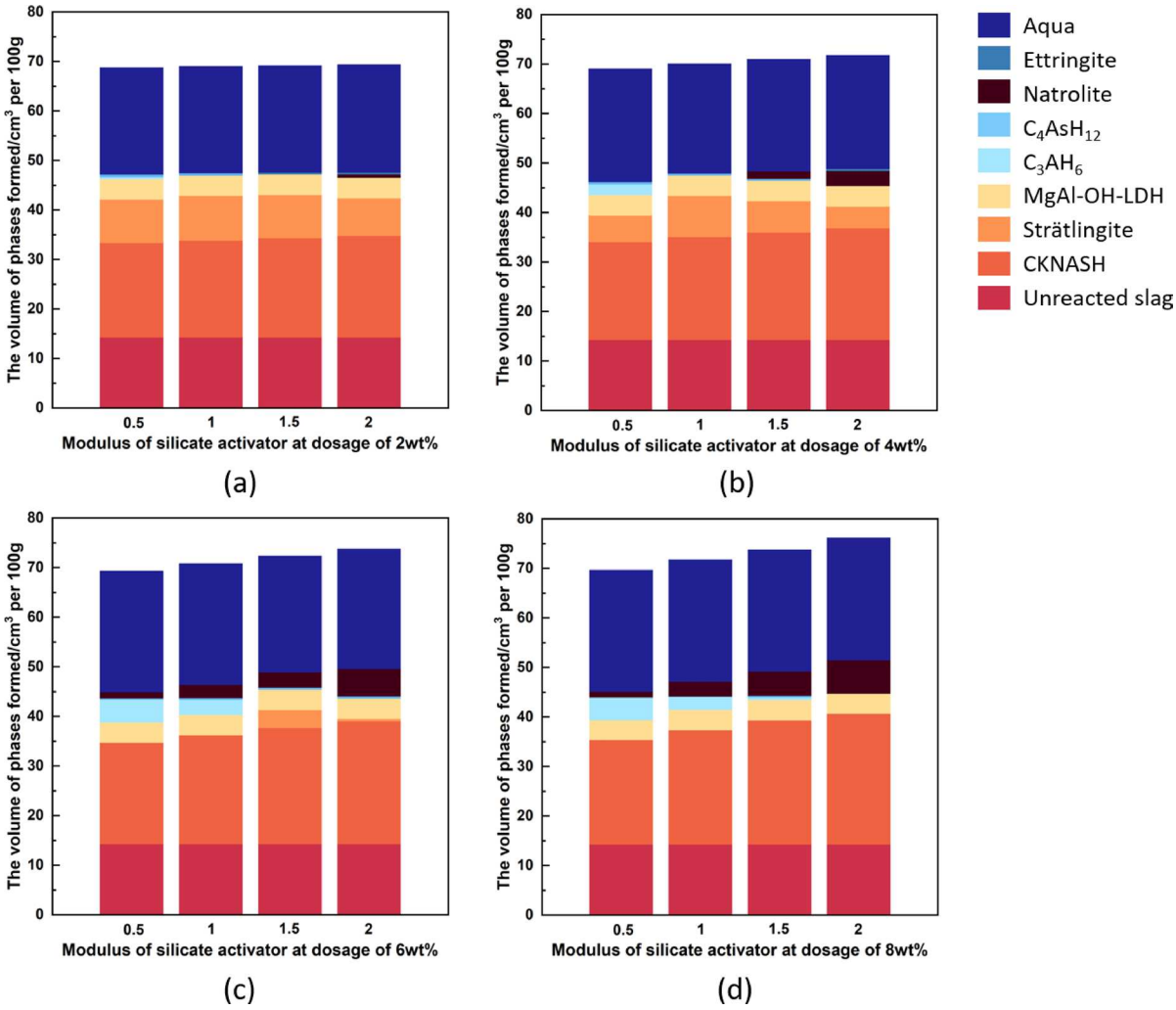

Fig. 2 The phase assemblage of GGBFS activated by different dosages of waterglass with various modulus values

kinetics when they are used as activators [39, 40], and are relatively less studied in terms of pore fluid chemistry. Lothenbach and Gruskovnjak [41] considered the degree of reaction of GGBFS and predicted the solution chemistry via thermodynamic modelling. Myers et al. [14] also simulated the concentrations of dissolved species in activated GGBFS binders using their C-N-A-S–H model and compared these with experimental results from the references above. In this study, the simulation trends are generally in agreement with the results of Lothenbach and Gruskovnjak, but the quantities are under-predicted [41]: the line representing the concentration of Ca is always at the lowest level while the increased trend for the concentration of Na can be seen as growing the dosage of activators. The reason for underestimation may be related to the experimental system not reaching equilibrium (i.e. an immature binder tested at early age) and the conservative degree of reaction of GGBFS used here (60%, compared to the 70–80% reacted in experiments [42]). However, the simulation results are still valuable for discussion of ASR, as this process takes quite a long time after hydration has largely stabilised.

Figure 4 displays the concentrations of Ca, K, Na and OH^- calculated to remain in the pore solution after hydration of GGBFS. The results for waterglass at 2% dosage with different modulus values

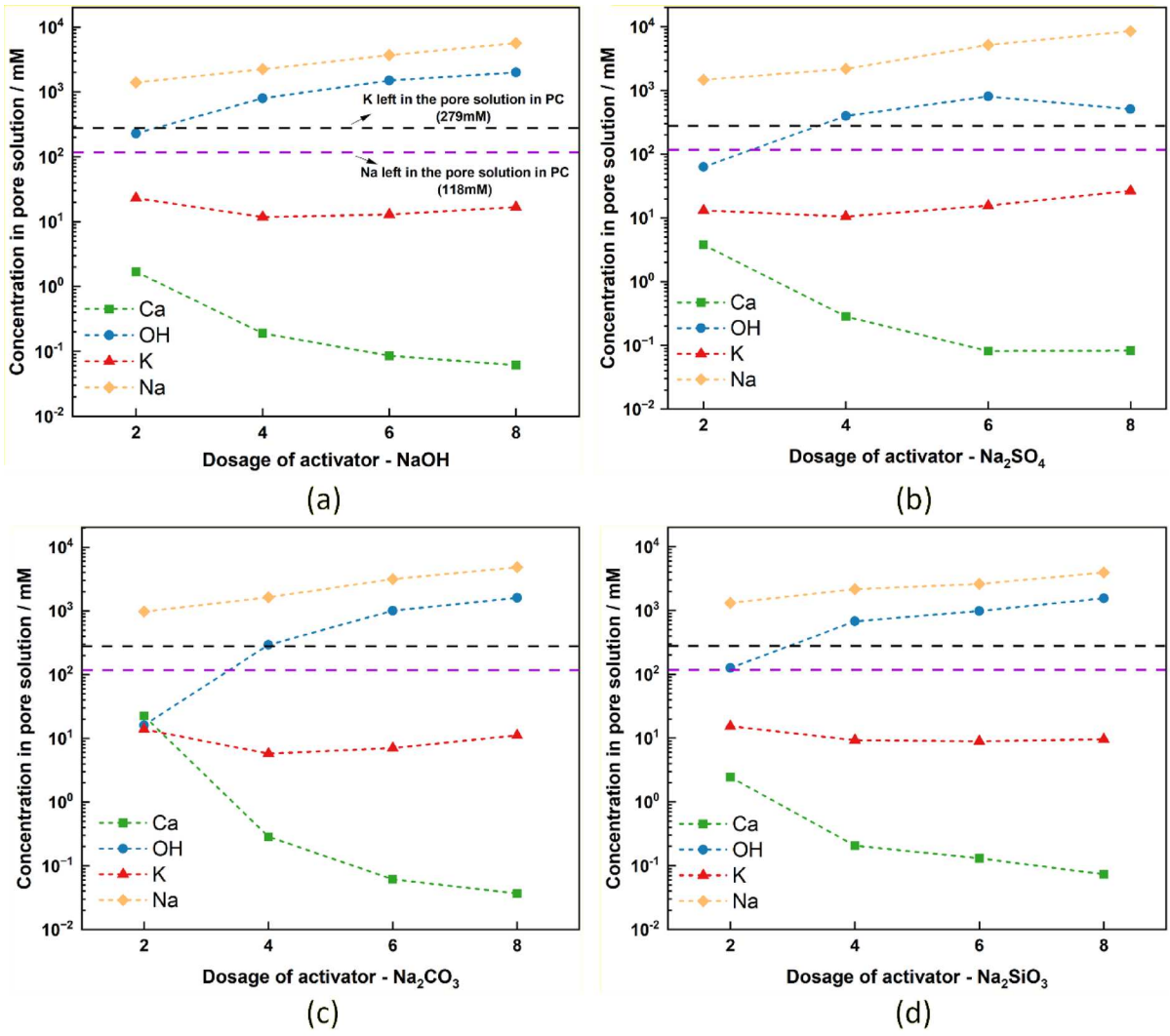

Fig. 3 The concentrations of Ca, K, Na and OH^- calculated to remain in the pore solution after hydration, for GGBFS activated by different dosages of four activators. Other anions such as sulfate that do not participate in ASR are not plotted. The two horizontal dashed lines represent the concentrations of K (black) and Na (purple) in the PC system

are shown here; the other dosages of silicate activators have similar trends. It can be seen that the concentration of Na decreases when increasing the modulus of waterglass, while the concentration of Ca increases, which is in agreement with the trends gained from experiments [43]. Combined with the results in Fig. 2 regarding the phase assemblage formed in each silicate-activated AAM, the fall in the concentration of K may be because the additional C-A-S–H formed at a higher modulus binds more K. Ca-bearing phases such as strätlingite, C_3AH_6 and C_4AsH_{12} formed at lower modulus are replaced by ettringite, as the sulfide from the slag becomes partially oxidised in the simulation. Therefore, this is main reason for the increase in the concentration of Ca in the pore solution shown in Fig. 4. The concentration of hydroxyl ions also decreases when the modulus of waterglass increases from 0.5 to 2 due to more soluble SiO_2 in the system, which acts as a polyprotic weak acid [44].

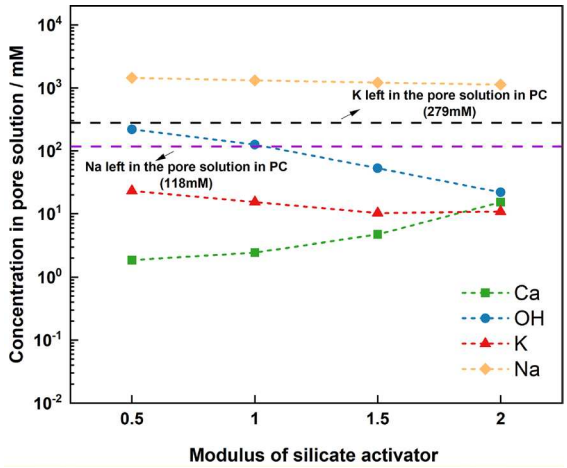

Fig. 4 The concentrations of Ca, K, Na and OH^- in the pore solution after activation of GGBFS by waterglass at different modulus values, at a dosage of 2% equivalent Na_2O. The two horizontal dash lines represent the concentrations of K (black) and Na (purple) in the PC system

3.3 ASR product formation

3.3.1 The effect of activator type and dosage on the volumes of ASR products formed

The volumes of two possible ASR products formed in the AAM system with four activators are shown in Table 4, with PC as a comparison. K-shlykovite only appears in the PC mortar; none of the AAMs precipitated this ASR product due to the lack of potassium in the composition of GGBFS. Na-shlykovite formed in some of the AAM simulations, but the volume of shlykovite-type products produced in all AAMs is much less than in the Portland cement mortar, regardless of the nature or dose of the activator. Na_2CO_3-activated GGBFS is the sample that contains the most Na-shlykovite compared with other AAM samples, forming almost 0.01 cm^3 per 100 g GGBFS.

According to the results of Chen et al., also considering the effect of type of activators on ASR, they observed the following order based on the ASR expansion experiments: waterglass, Na_2CO_3, Na_2SO_4, NaOH [45]. In the current study, however, the ranking of waterglass is changed, to come behind Na_2SO_4. The reason behind this may be because the modulus of waterglass in the Chen et al. study (3.29) was much higher than that in our modelling, which may provide an additional silica source when ASR is taking place. Krivenko et al. [3] also investigated the ASR expansion of GGBFS activated by sodium carbonate and sodium metasilicate, and found that Na_2CO_3-activated GGBFS is more affected by ASR than when the GGBFS is activated by sodium metasilicate. The modelling work is in agreement with these findings.

The simulation results here also support the idea that AAM has better performance in resisting ASR in comparison with PC, despite containing a much higher content of alkalis. Unlike the results of Talling and Brandstetr [6] who reported that there was no ASR expansion observed in AAMs, the findings presented here indicate that ASR can exist, but is less prevalent compared with the situation in PC [4, 5].

In terms of the effect of activator dose, the ASR product is only predicted to form when GGBFS is activated by activators with 2% equivalent Na_2O dosage (for all activators), and also when GGBFS is activated by the highest dosage of NaOH. In other words, increasing the dosage of activators does

Table 4 The effect of dosage on the volume of shlykovite-type products formed in the cement systems simulated, in cm^3 per 100 g GGBFS. The Na_2O_{eq} content of the Portland cement is taken from Table 1

$Na_2O_{(eq)}$	PC	NaOH	Na_2SiO_3**	Na_2CO_3	Na_2SO_4
2%	-	0.0030	0.0064	0.078	0.0096
4%	-	0	0	0	0
6%	-	0	0	0	0
8%	-	0.45	0	0	0
0.29 g per 100g PC	0.99 (0.72 K; 0.27 Na) *	-	-	-	-

* In all cases, the Na-shlykovite form dominates the ASR products, except for PC [19]

** The waterglass activation here is simulated with an activator modulus of 1.0, giving a composition of Na_2SiO_3

not directly increase the formation of ASR products in the cements studied here. When the dosage of NaOH increases to 8% of equivalent Na_2O, pH increases, resulting in the combination between Ca ion and hydroxyl ions, leading to portlandite precipitation which although minor (Fig. 1), needs to be considered in simulating the process of ASR [19]. This is the main reason for formation of more Na-shlykovite, as additional Ca becomes available for ASR processes. It should be noted that the two-step ASR simulation methodology applied here does not consider the C-S–H-type binding gels as a potential source of calcium for shlykovite formation, and so the only other Ca made available for this reaction is the residual Ca in the pore fluid after hydration.

Shi et al. [46, 47] concluded that the expansion caused by ASR decreased when increasing the concentration of NaOH from 4 wt% to 8 wt% in NaOH-activated GGBFS, which is incompatible with our simulation results. Similarly, the experimental results obtained from Yang's and Al-Otaibi's research also are conflicting with our predictions [48–50]. The difference between these findings may be attributed to testing methods and kinetic issues. For ASR research in AAMs, ASTM C1260 or similar rapid testing methods are often applied, in which expansion is determined after 14 days at high temperature immersed in NaOH solution [51]. However, here we simulate ASR under ambient temperature conditions and after AAM hydration, resulting in the binding of relevant ions in hydration products so that they no longer participate in the process of ASR, especially for calcium. The differences in temperature and highly alkaline immersion environment may also be important. Also, the conservative assumptions about the degree of reaction of GGBFS used in the modelling may mitigate the formation of more ASR products.

The results shown here seem to be supported by the previous work [18] where we generated and analysed the $(Na,K)_2O$-SiO_2-CaO ternary phase diagram to assess shlykovite stability and formation. That study concluded that the presence of more alkalis in the system does not necessarily improve the formation of shlykovite-type phases. Instead, there is a threshold concentration of alkali, which is less than 1.48 mol/kg. Increasing the dosage of activators here does lead to a growth in the concentration of alkalis in the pore solution, which may instead suppress the formation of Na-shlykovite.

3.3.2 *The effect of modulus and dosage of waterglass on ASR products*

The effects of modulus (molar ratio SiO_2/Na_2O) and dosage of waterglass on the simulated formation of ASR products are shown in Table 5. Similar to the results in Table 4, the formation of Na-shlykovite is only predicted at the lowest dosage (2%) for each given modulus. The volume of ASR product increases with an increase in the modulus at this dosage. Increasing in the modulus provides extra silica source to react with alkali ions and form ASR product. The experimental results are contradictory regarding this point. Tänzer et al. [2] presented the same trend as these simulation results, while Shi et. al [46] gained different outcomes with different waterglass dosages. At a lower dosage (4% Na_2O) there is a pessimum expansion when the modulus is 1, and similar trends are observed at dosages of 6% and 8% Na_2O. They attributed this to the alkalinity of the pore solution. However, the calculated concentrations of hydroxyl ions after AAM hydration reduced (Fig. 4), even at 4% equivalent Na_2O, which indicates that there must be another mechanism controlling this.

3.3.3 *Phases formed in the process of ASR*

Apart from Na-shlykovite, at the higher dosage and modulus of activators, zeolite-like phases (represented as natrolite) and Ca-heulandite are precipitated in minor amounts instead of ASR products. The rest of the dissolved silica either remains in the pore solution, or forms amorphous silica. Myers et al. [32] concluded that these two phases are prone to form in the

Table 5 The effect of modulus and dosage of waterglass on the quantity of Na-shlykovite formed in GGBFS activated by waterglass, expressed in cm^3/100 g GGBFS

SiO_2/Na_2O	2% Na_2O	4% Na_2O	6% Na_2O	8% Na_2O
0.5	0.0036	0	0	0
1.0	0.0064	0	0	0
1.5	0.015	0	0	0
2.0	0.053	0	0	0

alkali-activation of lower-Al, Si-rich slags. Although they are not predicted to form in the hydration modelling, the ASR process creates a similar environment, and this is an important reason for the suppression of the formation of ASR products. In addition, combining the information obtained here about the phase assemblages formed with different modulus values of waterglass at same dosage, it appears that increasing the modulus leads to precipitation of natrolite before the process of ASR, which consumes part of the Na from the pore solution. Therefore, the volume of this zeolite decreases in the second stage.

4 Discussion

Opinions on the performance of AAMs regarding ASR resistance are currently contradictory. In this study, the results from thermodynamic modelling indicate that a minor amount of ASR products formed in alkali-activated slag-based cements with different activators compared with PC. Although the actual degree of expansion caused by ASR depends on various factors such as the rate of reaction (dissolution) of the aggregate, viscosity and water uptake of ASR products, and density and mechanical properties of the paste, it is nonetheless important to consider the extent of ASR product formation as a prerequisite for any expansion to occur. Combining the pore solution chemistry and volume of ASR products shown in Fig. 3 and Table 4, due to the very limited availability of K in the AAMs, no K-shlykovite is predicted to form in these AAMs. The concentration of Na increases dramatically when using the four Na-bearing activators. Nevertheless, this higher concentration of Na in the pore solution does not result in the formation of more Na-shlykovite in the simulations: compared with NaOH- and Na_2CO_3-activated GGBFS at 2% equivalent Na_2O, the predicted concentration of Na in the former pore fluid (1400 mmol/L) is higher than in the latter (976 mmol/L), but the formation of Na-shlykovite in the Na_2CO_3-activated GGBFS was the greatest in simulations. This indicates that the concentration of alkalis in the pore solution is not the sole factor controlling the formation of ASR products.

In the work of Shi et al. [46], a linear relationship was observed between the concentration of hydroxyl ions and the ASR expansion, when considering different dosages of the activator. In the simulation methodology applied here, the concentration of OH^- appears to have at most an indirect impact on the formation of ASR products. This can be seen by comparison of activators: for Na_2SO_4- and Na_2CO_3-activated AAMs, the concentration of OH^- is lower than the other mixes because these two activators are near-neutral salts with less alkaline pH values, but the content of Na-shlykovite predicted to be formed in these two systems is higher than for the NaOH- and $Na_2O.nSiO_2$-activated formulations. Also, in terms of the effect of activator dosage, the concentration of hydroxyl ions increases to almost 2 mol/L when increasing the dosage of each activator to 8%. However, no Na-shlykovite forms even at such a high concentration of hydroxyl ions.

With respect to Ca, many studies have proven that the concentration of Ca in the pore solution plays an important role in the formation and composition of ASR products [25, 52–54]. The concentration of Ca in the pore fluids reaches a maximum with a 2% dosage of Na_2O, Fig. 3, consistent with the rank order of the volumes of Na-shlykovite predicted to form (Table 4), which always reaches a maximum at that dosage of 2% among those tested here. The higher the concentration of Ca left in the pore solution in AAM samples, the more Na-shlykovite is formed. Likewise, increasing the modulus of sodium silicate leads to an increase in the amount of Ca ions in the pore solution, which also leads to simulation of more ASR products forming. The higher activator dosages suppress Ca concentrations to the point where there is no longer any ASR product formed. It can be seen in Fig. 5, that in additional simulations with further reductions in the dosage of NaOH, the relationship between the concentration of Ca and the volume of ASR products is clearer: the lower the dosage used, the higher the concentration of Ca in the pore solution, and the more ASR products formed. This indicates that the lack of an available Ca source may result in the suppression of ASR product formation, even in these binders which do contain Ca in their hydrate phase assemblage, if that Ca is not available to redissolve and trigger an ASR process. The amorphous silica that dissolves from reactive aggregates may be soluble and left in the pore solution, or may react with alkalis to form zeolites or related phases in the absence of enough available Ca [55, 56]. It could be argued that the other Ca-containing phases present, such as C-A-S–H, may also provide a reservoir

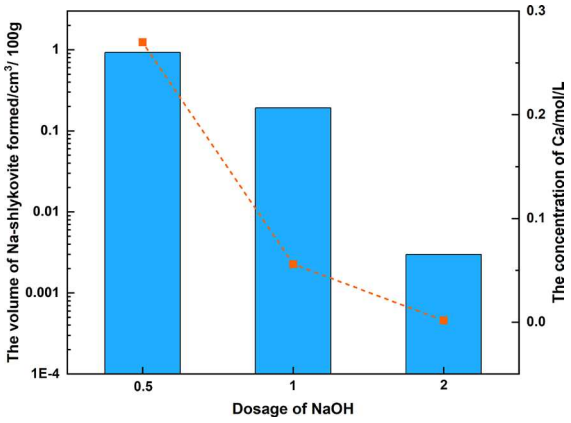

Fig. 5 The relationship between the concentration of Ca in the pore solution of AAM and the volume of Na-shlykovite formed in the process of ASR, with different dosages of NaOH. The dosages where no ASR products form are not displayed here

of available Ca for reaction, but it is likely that the Ca will be rather tightly held by C-A-S–H at the low Ca/Si ratios present in AAMs, so this potential pathway was not included in the simulation methodology here.

In comparison with the pore solution of Portland cement, the concentration of Ca remains higher for these four AAM samples. However, in the Portland cement system, portlandite ($Ca(OH)_2$) as one of the main hydration products provides most of the Ca required for ASR, in addition to the concentration of Ca in the pore solution. This indicates again that in this case, the Ca source rather than the alkali content in the pore solution is the key factor controlling the formation of ASR products. As in the case of the PC, the presence of $Ca(OH)_2$ in the highest-dosage NaOH-activated sample triggers the process of ASR and the formation of more ASR products. This can be used to explain the results in Table 4 where there is the highest volume of Na-shlykovite formed in this cement among all the AAMs simulated.

The role of Al in mitigating ASR in blended Portland cements is widely reported, and it can act either by slowing the dissolution of soluble silica from reactive aggregates [57, 58], or because it decreases the available alkali in the pore solution by dilution effects [16, 59, 60]. This inhibition is more notable in the presence of Al-rich supplementary cementitious materials such as metakaolin and fly ash. However, the analysis here focuses on GGBFS with intermediate Al content, and according to the phase assemblages shown in Fig. 1, most of the Al reacts with other ions to form hydrate phases rather than remaining available for interactions in ASR-related processes. Therefore, this study does not cover detailed discussion of the role of Al.

The simulation results here indicate that the restricted Ca availability, in conjunction with the alkali ions, has a greater influence on ASR than the higher alkalinity of the pore solution. The presence of less Ca in the AAM precursors such as GGBFS may become an advantage instead. Although experimental results do not often quantity the amount of ASR products, the relatively limited formation of shlykovite-type phases in AAM simulations supports the observed better performance in terms of ASR resistance for AAMs than PC.

5 Limitations and perspectives

The simulations here successfully predicted the formation of shlykovite-type ASR products in AAM systems with different activators. However, there exist some limitations that need to be clarified. Firstly, the predictions of ASR formation are difficult to compare with experiments, as there are few published testing methods that correspond to the conditions simulated; ASR testing is almost always conducted at elevated temperature, but we have focused here on ambient temperature to better represent field conditions. Therefore, more work should be done to investigate the amounts and details of any ASR products formed, ideally using long-term aged AAM samples. Also, the shlykovite-type ASR product is not the only possible type of ASR phases, but some others are not yet thermodynamically described, and so more of these types of product need to be included in the database. However, the aim of thermodynamic modelling as used here is to generate data that are difficult to obtain from experiments, but relatively more accessible by simulation. In terms of the database and future model development, the binding of alkalis by C-S–H type phases has been improved over the past decades by using different structural and sorption models, but there is still significant scope for improved understanding and description of both cation and anion

sorption on cementitious hydrate phases, which is a significant opportunity for future improvements in the outcomes of models such as the one presented here.

6 Conclusions

The development of thermodynamic modelling approaches based on an updated database for ASR products allows researchers to make comparison between experiment and modelling. In this study we investigated ASR in alkali-activated slag cements by changing the types, dosages, and modulus of activators (NaOH, Na_2SO_4, Na_2CO_3, Na_2SiO_3), using a two-step simulation method. The solution chemistry and phase assemblage after hydration were obtained and analysed to further explain the trends for the formation of ASR products. The conclusions are as follows:

(1) Compared with Portland cement, there is no K-shlykovite and much less Na-shlykovite formed in the simulations of alkali activated cement. Na-shlykovite was formed only with 0.5–2% and 8% equivalent Na_2O added as NaOH, and only formed at the lowest dosage simulated (2%) for the rest of the activators. For waterglass activation, the volume of ASR products increases when increasing the waterglass modulus.
(2) Combining the results of solution chemistry and phase assemblages, for those samples which form Na-shlykovite, the main reason for this is the higher concentration of Ca in the pore solution after hydration, and the formation of less potentially-reactive Ca-bearing hydration products. This reason can also apply for the silicate-activated GGBFS with different modulus values that influence the availability of soluble SiO_2. The concentration of alkali is not the sole controlling factor for the formation of ASR products, even though there is a much higher concentration of alkali in the pore solution of alkali-activated cement. Portlandite was found in the simulated phase assemblage when the dosage of NaOH increased to 8% equivalent Na_2O, which also triggers the process of ASR.

Acknowledgements This research did not receive any specific grant from funding agencies in the public, commercial, or not-for-profit sectors.

Author contributions **Haoliang Jin:** Conceptualization, Investigation, Methodology, Writing – original draft, Writing – review & editing. **Sam Ghazizadeh**: Methodology, Writing – review & editing. **John L. Provis**: Investigation, Methodology, Writing – review & editing.

Funding Open Access funding provided by Lib4RI – Library for the Research Institutes within the ETH Domain: Eawag, Empa, PSI & WSL.

Declarations

Conflict of interest The authors declare that they have no known competing financial interests or personal relationships that could have appeared to influence the work reported in this paper.

References

1. Bakharev T, Sanjayan JG, Cheng YB (2001) Resistance of alkali-activated slag concrete to alkali-aggregate reaction. Cem Concr Res 31:331–334. https://doi.org/10.1016/S0008-8846(03)00125-X
2. Tänzer R, Jin Y, Stephan D (2017) Effect of the inherent alkalis of alkali activated slag on the risk of alkali silica reaction. Cem Concr Res 98:82–90. https://doi.org/10.1016/j.cemconres.2017.04.009
3. Krivenko P, Drochytka R, Gelevera A, Kavalerova E (2014) Mechanism of preventing the alkali–aggregate reaction in alkali activated cement concretes. Cem Concr Compos 45:157–165. https://doi.org/10.1016/j.cemconcomp.2013.10.003
4. Gifford PM, Gillott JE (1996) Alkali-silica reaction (ASR) and alkali-carbonate reaction (ACR) in activated blast furnace slag cement (ABFSC) concrete. Cem Concr Res 26:21–26
5. García-Lodeiro I, Palomo A, Fernández-Jiménez A (2007) Alkali–aggregate reaction in activated fly ash systems.

Cem Concr Res 37:175–183. https://doi.org/10.1016/j.cemconres.2006.11.002
6. Talling B, Brandstetr J (1989) Present state and future of alkali-activated slag concretes. ACI Spec Publ 114:1519–1546
7. Wang W, Noguchi T, Maruyama I (2022) Mechanism understanding of alkali-silica reaction in alkali-activated materials system. Cem Concr Res 156:106768. https://doi.org/10.1016/j.cemconres.2022.106768
8. Shi C, Shi Z, Hu X, Zhao R, Chong L (2015) A review on alkali-aggregate reactions in alkali-activated mortars/concretes made with alkali-reactive aggregates. Mater Struct 48:621–628. https://doi.org/10.1617/s11527-014-0505-2
9. Wang W, Noguchi T (2020) Alkali-silica reaction (ASR) in the alkali-activated cement (AAC) system: a state-of-the-art review. Constr Build Mater 252:119105. https://doi.org/10.1016/j.conbuildmat.2020.119105
10. Alexandre R, Josée D, Benoit F, Mathieu C, Benoit B (2020) Alkali-silica reaction in alkali-activated combined slag and fly ash concretes: The tempering effect of fly ash on expansion and cracking. Constr Build Mater 251:118968. https://doi.org/10.1016/j.conbuildmat.2020.118968
11. Winnefeld F, Gluth GJG, Bernal SA, Bignozzi MC, Carabba L, Chithiraputhiran S, Dehghan A, Dolenec S, Dombrowski-Daube K, Dubey A, Ducman V, Jin Y, Peterson K, Stephan D, Provis JL (2020) RILEM TC 247-DTA round robin test: sulfate resistance, alkali-silica reaction and freeze–thaw resistance of alkali-activated concretes. Mater Struct 53:140. https://doi.org/10.1617/s11527-020-01562-0
12. Lothenbach B (2010) Thermodynamic equilibrium calculations in cementitious systems. Mater Struct 43:1413–1433. https://doi.org/10.1617/s11527-010-9592-x
13. Lothenbach B, Zajac M (2019) Application of thermodynamic modelling to hydrated cements. Cem Concr Res 123:105779. https://doi.org/10.1016/j.cemconres.2019.105779
14. Myers RJ, Bernal SA, Provis JL (2014) A thermodynamic model for C-(N-)A-S-H gel: CNASH_ss. derivation and validation. Cem Concr Res 66:27–47. https://doi.org/10.1016/J.CEMCONRES.2014.07.005
15. Kulik DA, Miron GD, Lothenbach B (2022) A structurally-consistent CASH+ sublattice solid solution model for fully hydrated C-S-H phases: thermodynamic basis, methods, and Ca-Si-H_2O core sub-model. Cem Concr Res 151:106585. https://doi.org/10.1016/j.cemconres.2021.106585
16. L'Hôpital E, Lothenbach B, Scrivener K, Kulik DA (2016) Alkali uptake in calcium alumina silicate hydrate (C-A-S-H). Cem Concr Res 85:122–136. https://doi.org/10.1016/j.cemconres.2016.03.009
17. Shi Z, Geng G, Leemann A, Lothenbach B (2019) Synthesis, characterization, and water uptake property of alkali-silica reaction products. Cem Concr Res 121:58–71. https://doi.org/10.1016/j.cemconres.2019.04.009
18. Jin H, Ghazizadeh S, Provis JL (2023) Assessment of the thermodynamics of Na,K-shlykovite as potential alkali-silica reaction products in the $(Na,K)_2O$-CaO–SiO_2-H_2O system. Cem Concr Res 172:107253. https://doi.org/10.1016/j.cemconres.2023.107253
19. Jin H, Ghazizadeh S, Provis JL (2024) Thermodynamic modelling of alkali-silica reactions in blended cements. Cem Concr Res 181:107543
20. Razki S, Benboudjema F, Bourdot A, Langlois S, Fau A, Hafid F, Honorio T (2025) Crystallization pressure in ASR expansion quantified by thermodynamic modeling and micromechanics. Cem Concr Res 193:107878. https://doi.org/10.1016/j.cemconres.2025.107878
21. Mundra S, Prentice DP, Bernal SA, Provis JL (2020) Modelling chloride transport in alkali-activated slags. Cem Concr Res 130:106011. https://doi.org/10.1016/j.cemconres.2020.106011
22. Duchesne J, Bérubé M-A (2001) Long-term effectiveness of supplementary cementing materials against alkali–silica reaction. Cem Concr Res 31:1057–1063. https://doi.org/10.1016/S0008-8846(01)00538-5
23. Kulik DA, Wagner T, Dmytrieva SV, Kosakowski G, Hingerl FF, Chudnenko KV, Berner UR (2013) GEM-Selektor geochemical modeling package: revised algorithm and GEMS3K numerical kernel for coupled simulation codes. Comput Geosci 17:1–24. https://doi.org/10.1007/s10596-012-9310-6
24. Helgeson H, Kirkham DH, Flowers GC (1981) Theoretical prediction of the thermodynamic behavior of aqueous electrolytes by high pressures and temperatures; IV, calculation of activity coefficients, osmotic coefficients, and apparent molal and standard and relative partial molal properties to 600°C and 5kb. Am J Sci 281:1249–1516
25. Chatterji S (1979) The role of $Ca(OH)_2$ in the breakdown of Portland cement concrete due to alkali-silica reaction. Cem Concr Res 9:185–188. https://doi.org/10.1016/0008-8846(79)90024-3
26. Hou X, Struble LJ, Kirkpatrick RJ (2004) Formation of ASR gel and the roles of C-S-H and portlandite. Cem Concr Res 34:1683–1696. https://doi.org/10.1016/j.cemconres.2004.03.026
27. Lothenbach B, Kulik DA, Matschei T, Balonis M, Baquerizo L, Dilnesa B, Miron GD, Myers RJ (2019) Cemdata18: a chemical thermodynamic database for hydrated Portland cements and alkali-activated materials. Cem Concr Res 115:472–506. https://doi.org/10.1016/j.cemconres.2018.04.018
28. Dilnesa BZ, Lothenbach B, Renaudin G, Wichser A, Kulik D (2014) Synthesis and characterization of hydrogarnet $Ca_3(Al_xFe_{1-x})_2(SiO_4)_y(OH)_{4(3-y)}$. Cem Concr Res 59:96–111. https://doi.org/10.1016/j.cemconres.2014.02.001
29. Matschei T, Lothenbach B, Glasser FP (2007) Thermodynamic properties of Portland cement hydrates in the system CaO–Al_2O_3–SiO_2–$CaSO_4$–$CaCO_3$–H_2O. Cem Concr Res 37:1379–1410. https://doi.org/10.1016/j.cemconres.2007.06.002
30. Ben Haha M, Le Saout G, Winnefeld F, Lothenbach B (2011) Influence of activator type on hydration kinetics, hydrate assemblage and microstructural development of alkali activated blast-furnace slags. Cem Concr Res 41:301–310. https://doi.org/10.1016/j.cemconres.2010.11.016
31. Richardson IG, Brough AR, Groves GW, Dobson CM (1994) The characterization of hardened alkali-activated blast-furnace slag pastes and the nature of the calcium

silicate hydrate (C-S-H) phase. Cem Concr Res 24:813–829. https://doi.org/10.1016/0008-8846(94)90002-7
32. Myers RJ, Bernal SA, Provis JL (2017) Phase diagrams for alkali-activated slag binders. Cem Concr Res 95:30–38. https://doi.org/10.1016/j.cemconres.2017.02.006
33. Myers RJ, Lothenbach B, Bernal SA, Provis JL (2015) Thermodynamic modelling of alkali-activated slag cements. Appl Geochem 61:233–247. https://doi.org/10.1016/j.apgeochem.2015.06.006
34. Lothenbach B, Matschei T, Möschner G, Glasser FP (2008) Thermodynamic modelling of the effect of temperature on the hydration and porosity of Portland cement. Cem Concr Res 38:1–18. https://doi.org/10.1016/J.CEMCONRES.2007.08.017
35. Dai X, Aydin S, Yardimci MY, Lesage K, De Schutter G (2022) Early age reaction, rheological properties and pore solution chemistry of NaOH-activated slag mixtures. Cem Concr Compos 133:104715. https://doi.org/10.1016/j.cemconcomp.2022.104715
36. Song S, Jennings HM (1999) Pore solution chemistry of alkali-activated ground granulated blast-furnace slag. Cem Concr Res 29(2):159–170
37. Puertas F, Fernández-Jiménez A, Blanco-Varela MT (2004) Pore solution in alkali-activated slag cement pastes. Relation to the composition and structure of calcium silicate hydrate. Cem Concr Res 34:139–148. https://doi.org/10.1016/S0008-8846(03)00254-0
38. Lloyd RR, Provis JL, Van Deventer JSJ (2010) Pore solution composition and alkali diffusion in inorganic polymer cement. Cem Concr Res 40:1386–1392. https://doi.org/10.1016/j.cemconres.2010.04.008
39. Bernal SA, Provis JL, Myers RJ, San Nicolas R, van Deventer JSJ (2015) Role of carbonates in the chemical evolution of sodium carbonate-activated slag binders. Mater Struct 48:517–529. https://doi.org/10.1617/s11527-014-0412-6
40. Rashad AM, Bai Y, Basheer PAM, Milestone NB, Collier NC (2013) Hydration and properties of sodium sulfate activated slag. Cem Concr Compos 37:20–29. https://doi.org/10.1016/j.cemconcomp.2012.12.010
41. Lothenbach B, Gruskovnjak A (2007) Hydration of alkali-activated slag: thermodynamic modelling. Adv Cem Res 19:81–92. https://doi.org/10.1680/adcr.2007.19.2.81
42. Durdziński PT, Ben Haha M, Bernal SA, De Belie N, Gruyaert E, Lothenbach B, Menéndez Méndez E, Provis JL, Schöler A, Stabler C, Tan Z, Villagrán Zaccardi Y, Vollpracht A, Winnefeld F, Zając M, Scrivener KL (2017) Outcomes of the RILEM round robin on degree of reaction of slag and fly ash in blended cements. Mater Struct 50:135. https://doi.org/10.1617/s11527-017-1002-1
43. Zuo Y, Nedeljković M, Ye G (2019) Pore solution composition of alkali-activated slag/fly ash pastes. Cem Concr Res 115:230–250. https://doi.org/10.1016/j.cemconres.2018.10.010
44. Swaddle TW (2001) Silicate complexes of aluminum(III) in aqueous systems. Coord Chem Rev 219–221:665–686. https://doi.org/10.1016/S0010-8545(01)00362-9
45. Chen YZ, Pu XC, Yang CH, Ding QJ (2002) Alkali aggregate reaction in alkali slag cement mortars. J Wuhan Univ Technol Mater Sci Ed 17:3–6. https://doi.org/10.1007/bf02838542
46. Shi Z, Shi C, Wan S, Zhang Z (2018) Effects of alkali dosage and silicate modulus on alkali-silica reaction in alkali-activated slag mortars. Cem Concr Res 111:104–115. https://doi.org/10.1016/j.cemconres.2018.06.005
47. Shi Z, Shi C, Zhao R, Wan S (2015) Comparison of alkali–silica reactions in alkali-activated slag and Portland cement mortars. Mater Struct 48:743–751. https://doi.org/10.1617/s11527-015-0535-4
48. Yang C, Pu X, Wu F (1999) A study on alkali-aggregate reaction of alkali-clinker-slag cement concrete. J Chongqing Jianzhu Univ 21:14–19
49. Yang C, Pu X, Wu F (1999) Research on alkali aggregate reaction expansion of alkali-slag mortar. J Chin Ceram Soc 1304:651–657
50. Al-Otaibi S (2008) Durability of concrete incorporating GGBS activated by water-glass. Constr Build Mater 22:2059–2067. https://doi.org/10.1016/j.conbuildmat.2007.07.023
51. ASTM, ASTM C1260: Standard test method for potential alkali reactivity of aggregates (mortar–bar method), ASTM International (2023).
52. Guo S, Dai Q, Si R (2019) Effect of calcium and lithium on alkali-silica reaction kinetics and phase development. Cem Concr Res 115:220–229. https://doi.org/10.1016/j.cemconres.2018.10.007
53. Kim T, Olek J, Jeong HG (2015) Alkali-silica reaction: kinetics of chemistry of pore solution and calcium hydroxide content in cementitious system. Cem Concr Res 71:36–45. https://doi.org/10.1016/j.cemconres.2015.01.017
54. Leemann A, Le Saout G, Winnefeld F, Rentsch D, Lothenbach B (2011) Alkali-silica reaction: The Influence of calcium on silica dissolution and the formation of reaction products. J Am Ceram Soc 94:1243–1249. https://doi.org/10.1111/J.1551-2916.2010.04202.X
55. D. Diamond, ASR - another look at mechanisms, Proceedings of the 8th International Conference on Alkali-Aggregate Reactions in Concrete, Kyoto, Japan, Eds.K Okada, S. Nishibayashi, M.Kawamura, ICAAR. (1989) 83–94.
56. J.P. Skalny, J. Gebauer, I. Odler, Materials Science of Concrete, Special Volume: Calcium Hydroxide in Concrete, John Wiley & Sons, 2001.
57. Bickmore BR, Nagy KL, Gray AK, Brinkerhoff AR (2006) The effect of $Al(OH)_4^-$ on the dissolution rate of quartz. Geochim Cosmochim Acta 70:290–305. https://doi.org/10.1016/j.gca.2005.09.017
58. Shi Z, Ma B, Lothenbach B (2021) Effect of Al on the formation and structure of alkali-silica reaction products. Cem Concr Res 140:106311. https://doi.org/10.1016/j.cemconres.2020.106311
59. Chappex T, Scrivener K (2012) Alkali fixation of C-S-H in blended cement pastes and its relation to alkali silica reaction. Cem Concr Res 42:1049–1054. https://doi.org/10.1016/j.cemconres.2012.03.010
60. Chappex T, Scrivener KL (2012) The influence of aluminium on the dissolution of amorphous silica and its relation to alkali silica reaction. Cem Concr Res 42:1645–1649. https://doi.org/10.1016/j.cemconres.2012.09.009